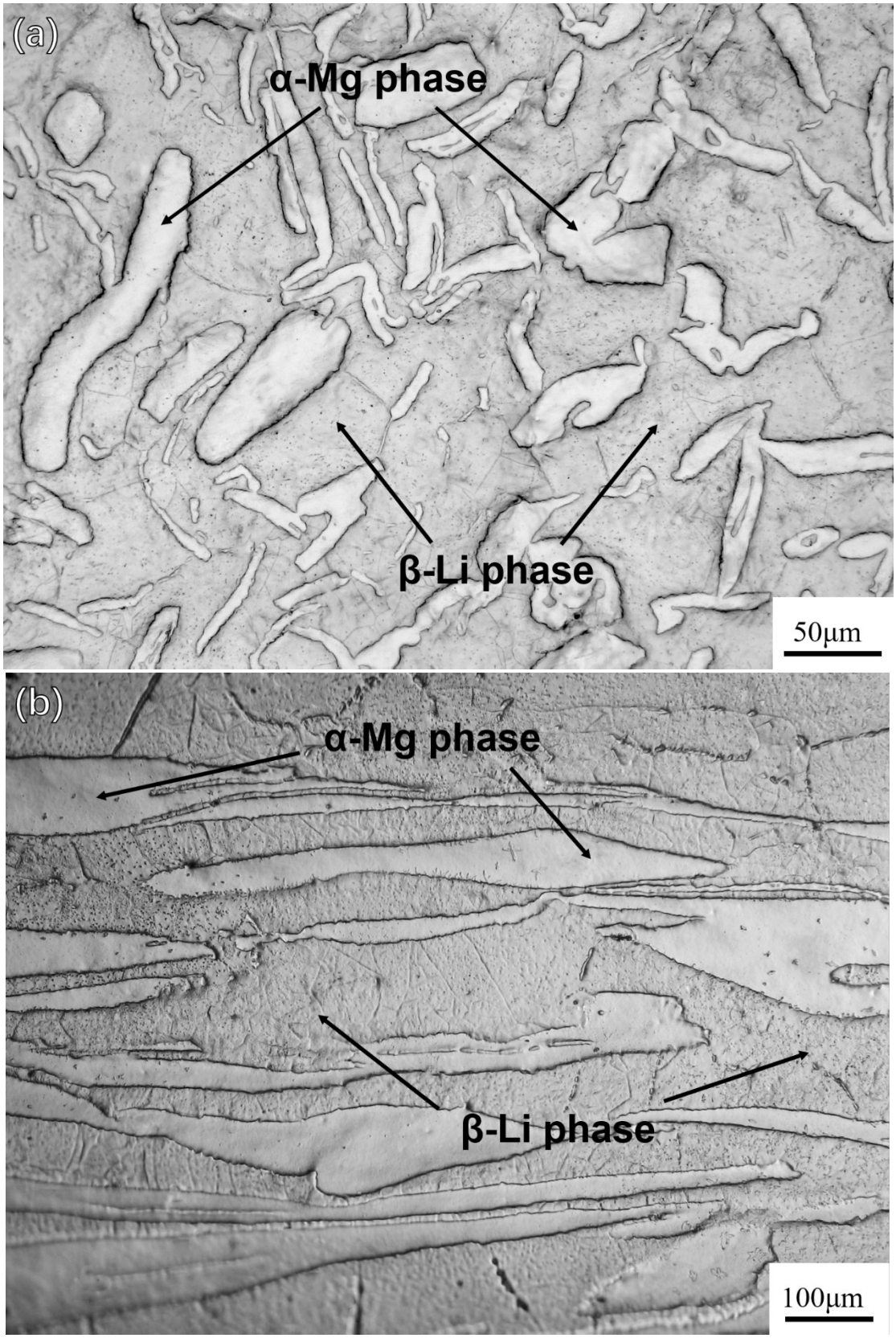

Figure 1. Microstructures of (a) cross-section and (b) side surface of the dual-phase LZ91 alloy

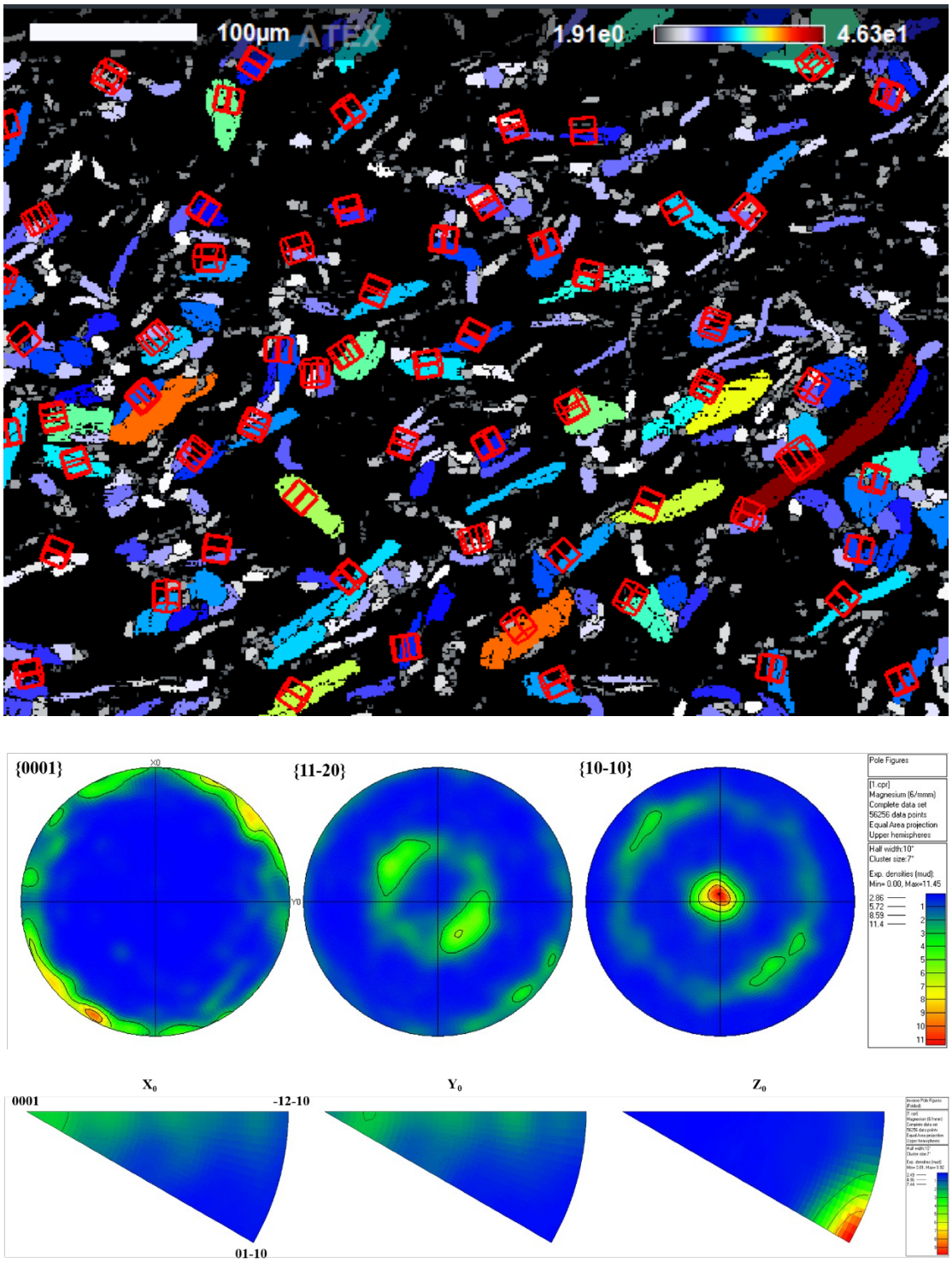

Fig. 2 Grain orientation information of the LZ91 alloy

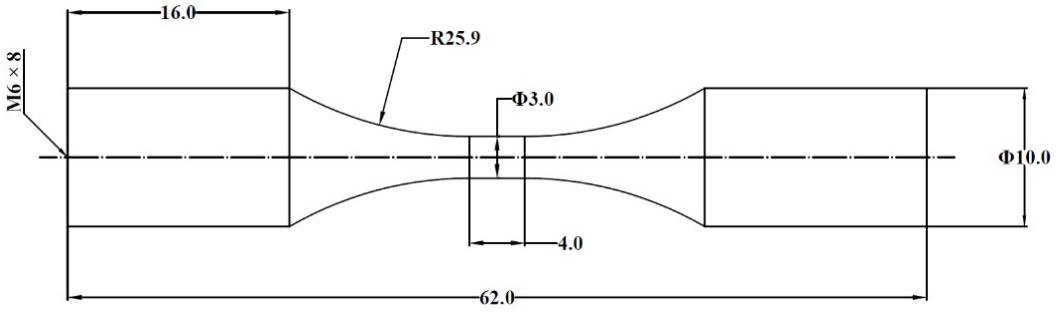

Figure 3. Specimen geometry for ultrasonic fatigue tests (unit: mm).

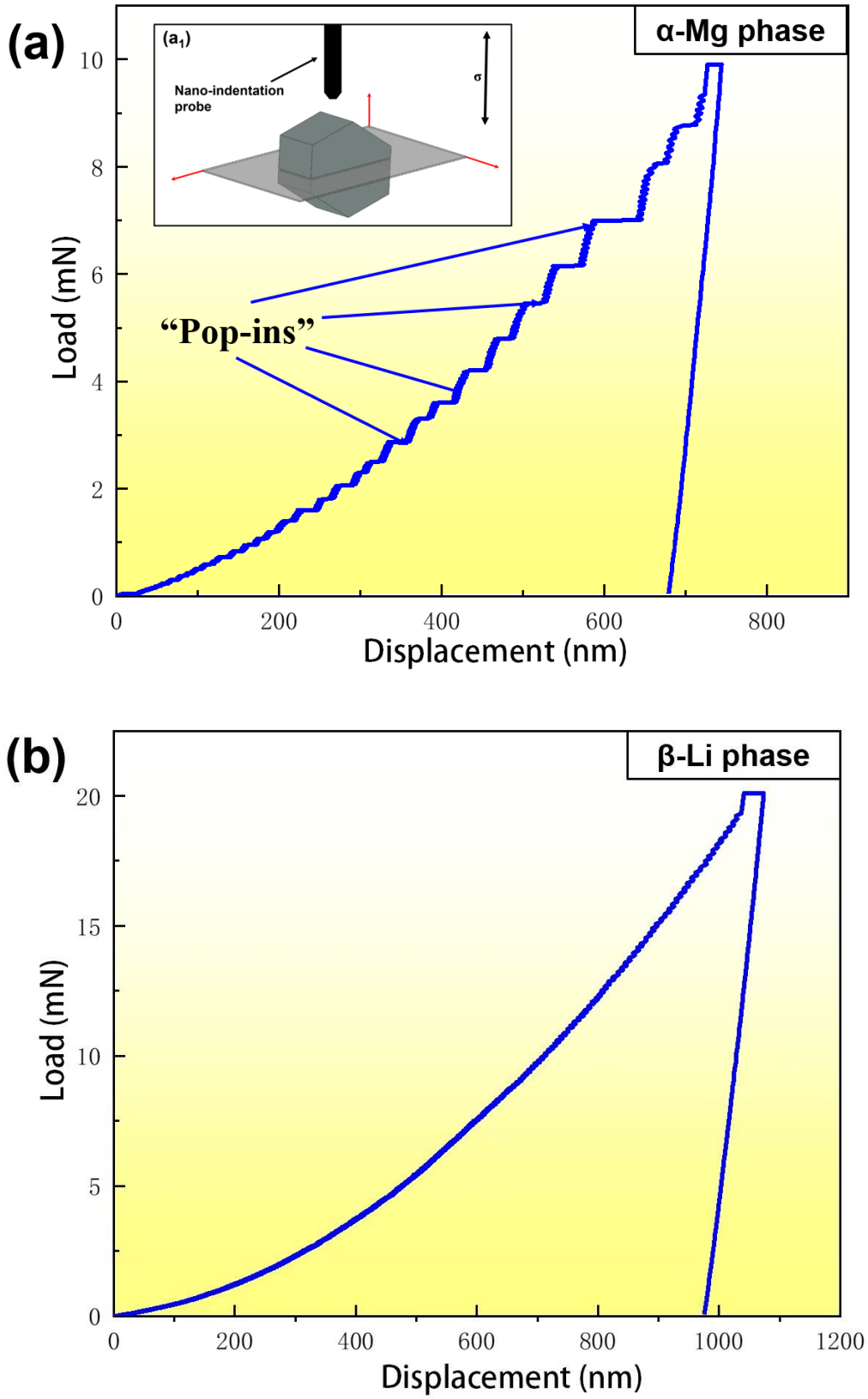

Figure 4. Nano-indentation results of (a) α-Mg phase and (b) β-Li phase, and (a_1) a schematic diagram of the force imposed by the probe on α-Mg grain.

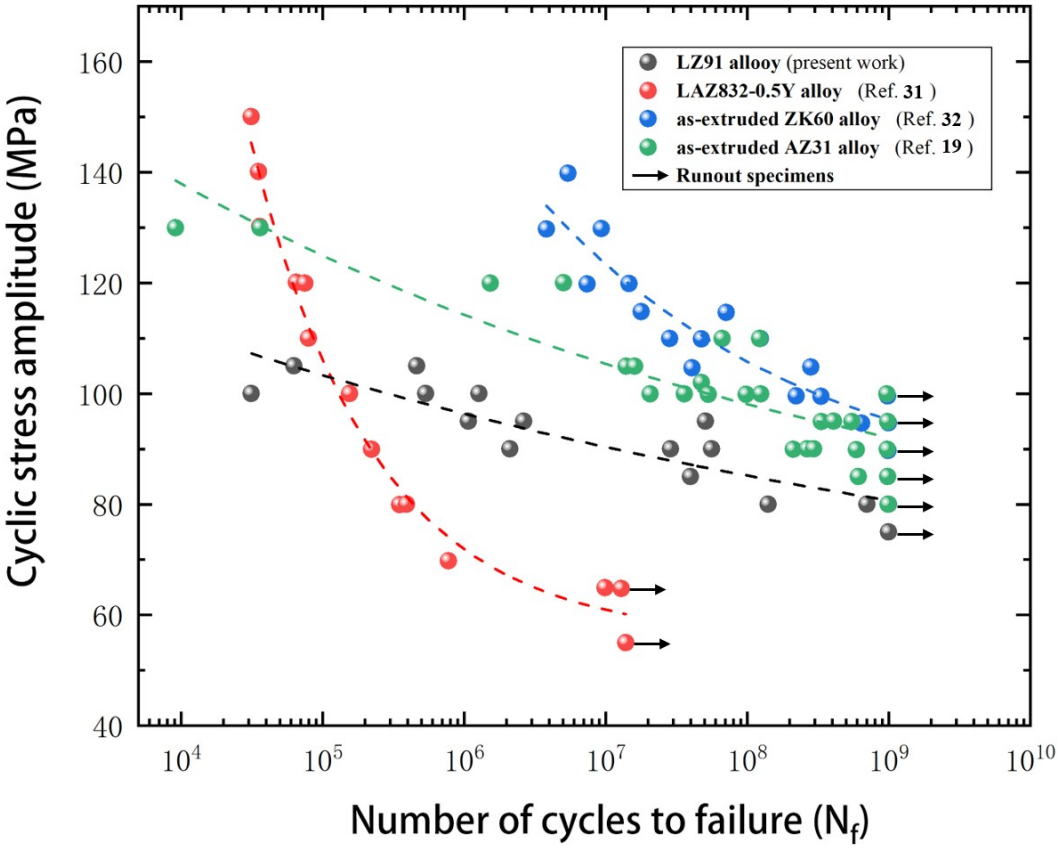

Figure 5. S-N data

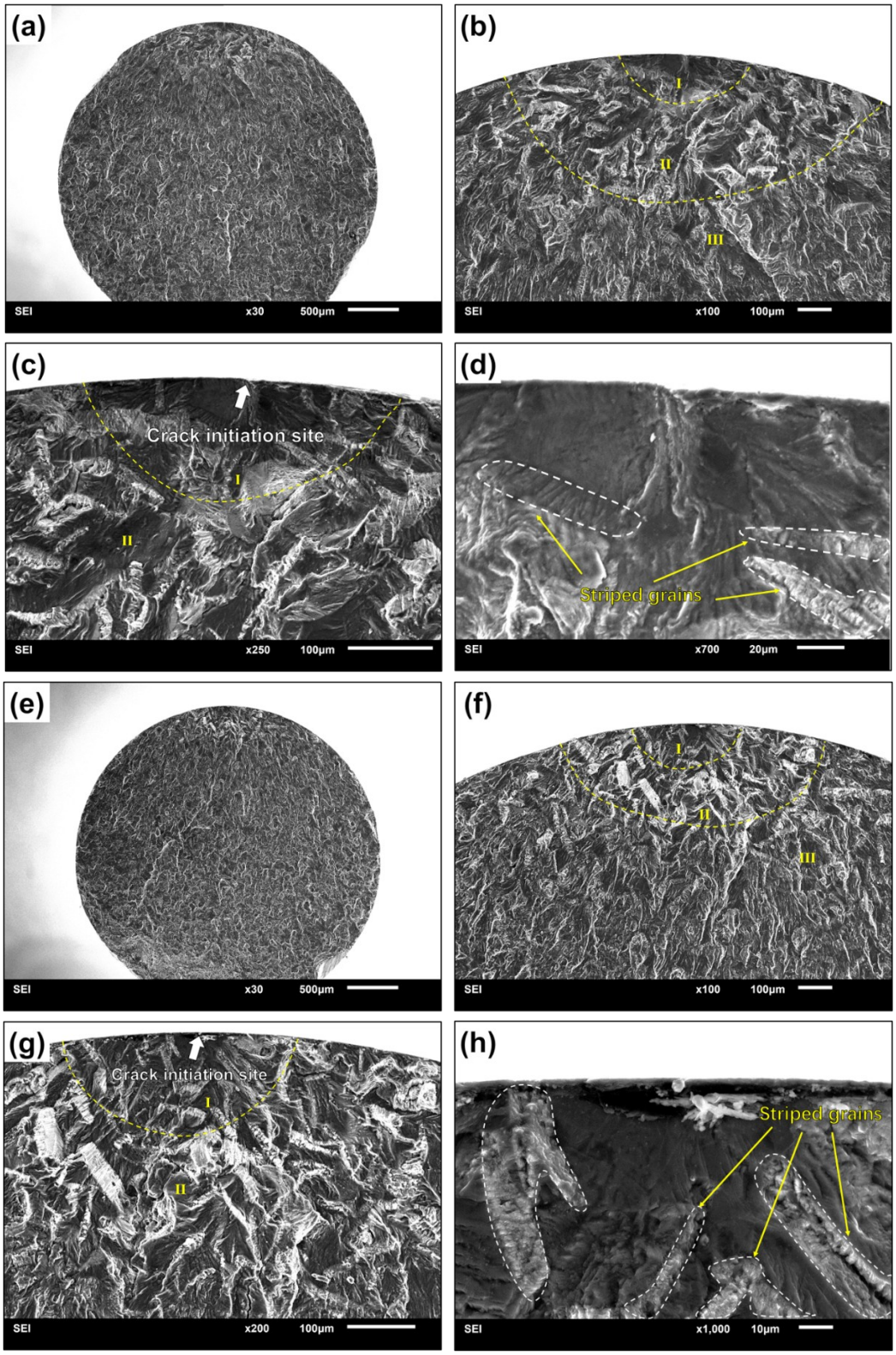

Figure 6. Typical fracture morphology of LZ91 Mg-Li alloy with surface crack initiation at a stress ratio of R = -1. (a): σ_a = 90 MPa $N_f = 2.88 \times 10^7$;and (b-d) enlarged images of crack initiation site in (a) at different magnifications; (e) σ_a = 90 MPa, $N_f = 1.16 \times 10^6$, and (f-h) enlarged images of crack initiation site in (e) at different magnifications.

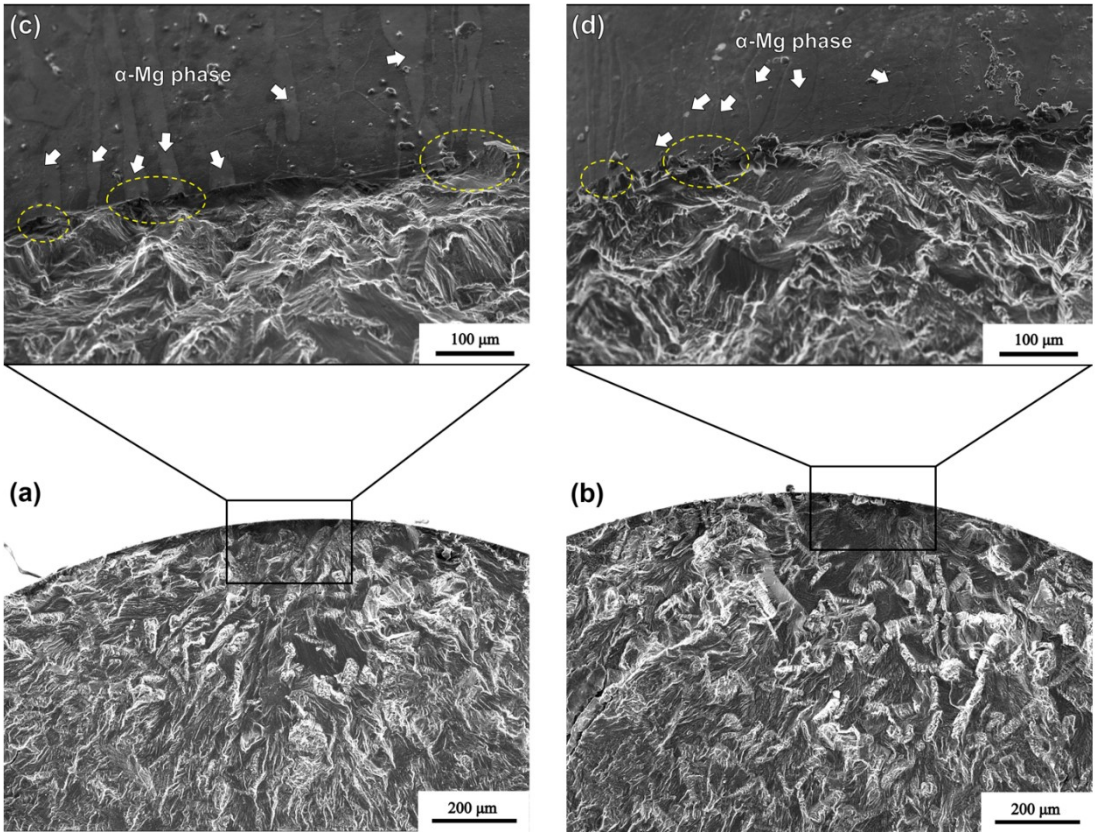

Figure 7. Morphology of (a) the fracture morphology of the crack initiation site, and (b) the corresponding morphology of the specimen surface

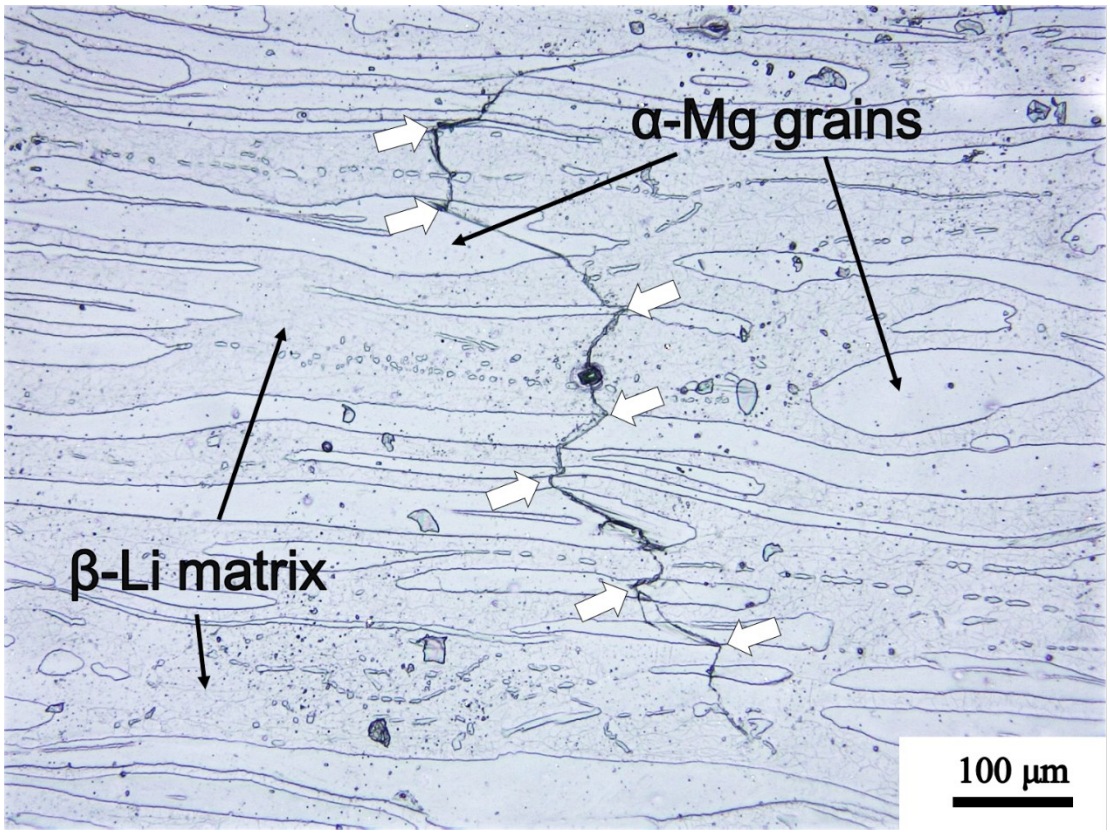

Figure 8. Optical image of a second crack on the specimen surface near the fracture

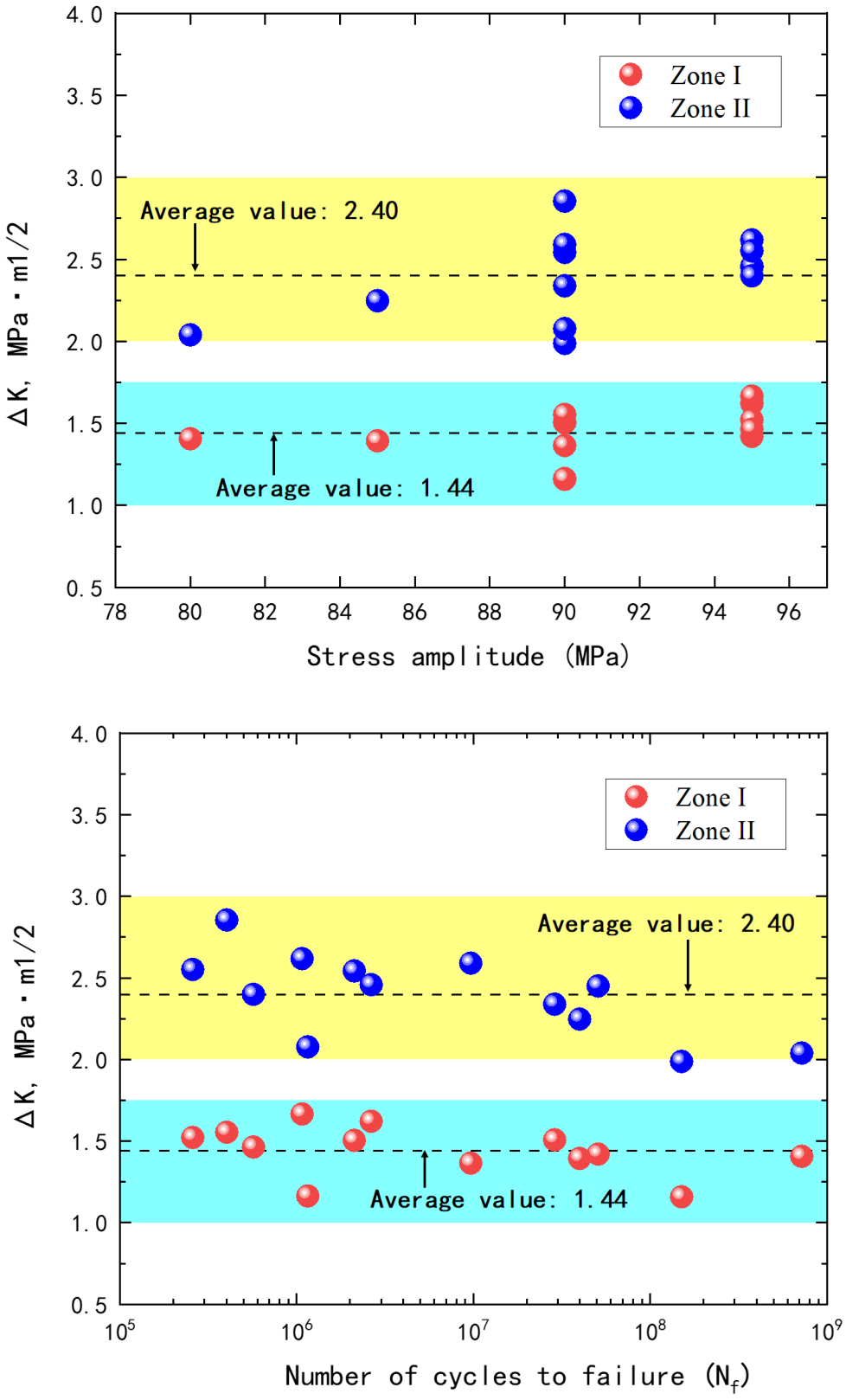

Figure 9. Relationship between stress intensity factor range ΔK and (a): fatigue strength; (b): fatigue life.

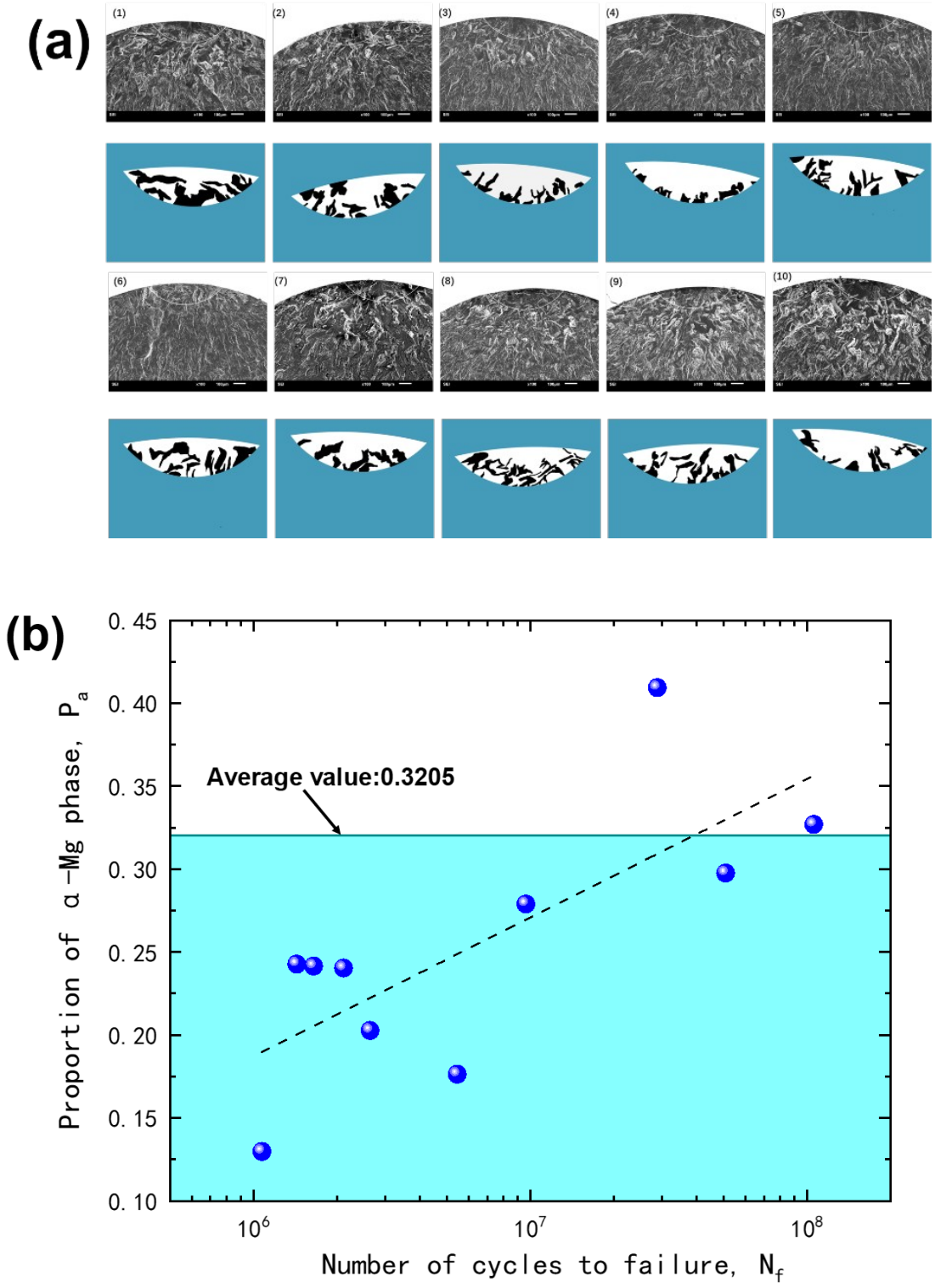

Figure 10. Morphology statistics of the region near the crack initiation site. (a): The calculated regions and the area occupied by α-Mg grains (in black); (b): Relation between the proportion of α-Mg phase and the fatigue life in the calculated regions.

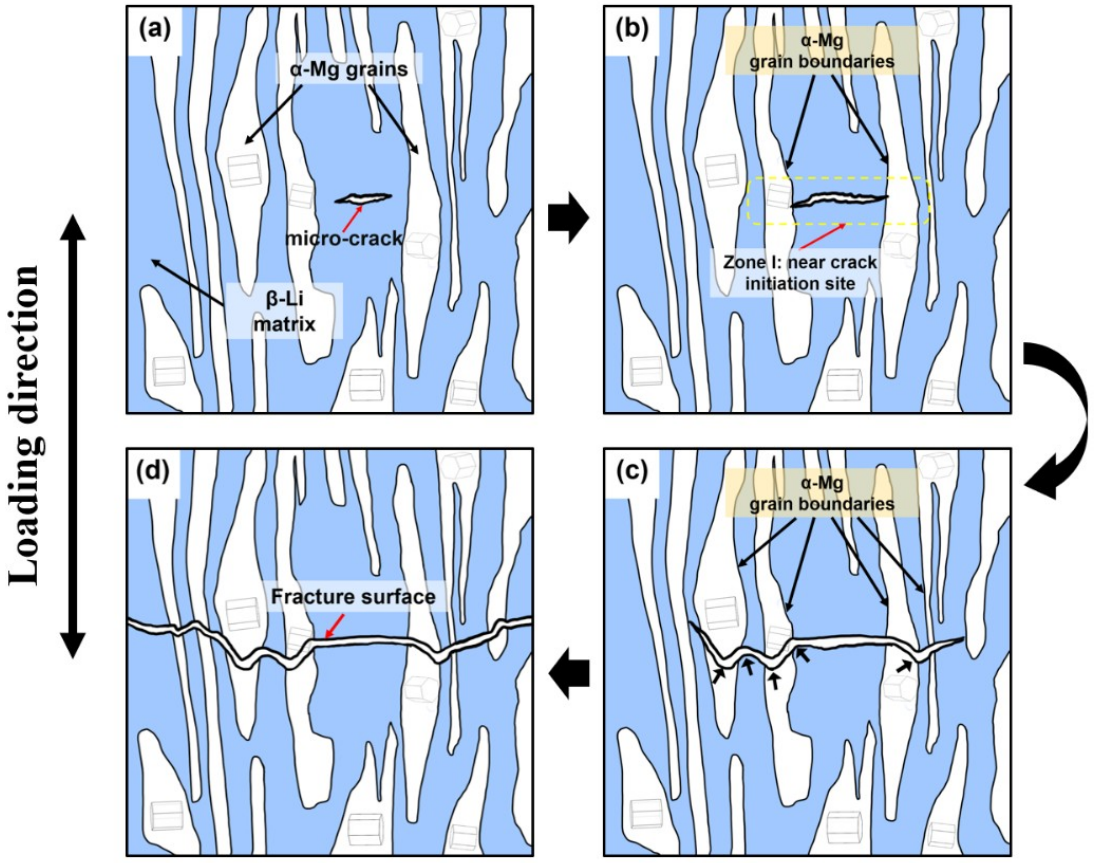

Figure 11. Schematic diagram of crack initiation and propagation.